Chapter 1

Electromagnetic scattering by fractal screens: from diffraction integrals towards a boundary element method

J. M. Christian[1] **and E. A. Chadwick**[2]

[1] Joule Physics Laboratory,
University of Salford, Greater Manchester M5 4WT.
j.christian@salford.ac.uk

[2] Mathematics,
University of Salford, Greater Manchester M5 4WT.
e.a.chadwick@salford.ac.uk

Abstract. *The scattering of time-harmonic electromagnetic fields by perfectly-conducting plane screens is a fundamental problem in physics. A standard approach to computing the scattered wave is to deploy Rayleigh-Sommerfeld diffraction integrals in conjunction with the ad hoc St. Venant hypothesis to enforce on-screen boundary conditions. These formulations are best suited to high-frequency regimes, where the characteristic aperture size a is typically much larger than the wavelength $\lambda = 2\pi/k$ such that $ka \gg 1$. They are also desirable because the well-known Fresnel (near field) and Fraunhofer (far field) integrals follow straightforwardly from Taylor expansions within the Rayleigh-Sommerfeld kernel. However, diffraction integrals must be used with caution when the screen has some kind of fractal (or self-similar) structure—for example, those based on a finite number of stages in the Cantor set or Sierpinski triangle. In such cases, the low-frequency regime $ka \ll 1$ may be encountered as a matter of course.*

A more rigorous approach is to consider scattering as a formal boundary-value problem for the underlying Helmholtz equation. One constructs a boundary integral equation with reference to the free Green's function, then discretizes the domain of the screen to arrive at a corresponding boundary element formulation. In this way, boundary conditions (typically either Dirichlet or Neumann) are accommodated as a natural part of the numerical scheme. The key advantage over diffraction integrals is that low-frequency regimes can be accessed without difficulty. Our presentation will survey earlier results obtained from a Rayleigh-Sommerfeld prescription, providing background and context. A new boundary element formulation will then be detailed along with some preliminary results.

1.1 Introduction

Formulations of wave diffraction problems in terms of Rayleigh-Sommerfeld integrals, while not mathematically rigorous, remain legitimate theoretical approaches [1, 2]. Supporting evidence for their validity can be found in laser optics experiments, where measurements are often in excellent agreement with theory (especially in the far field) [3]. While the assumptions underpinning diffraction integrals should always be borne in mind, particular care must be taken when scatterers are pre-fractal or fractal in nature [4, 5, 6]. In the context of transparent apertures made in otherwise opaque plane screens, diffraction integrals tend to work best when the largest characteristic size a of the constituent apertures is much greater than the wavelength $\lambda = 2\pi/k$ of the incident wave. This scenario is the high-frequency regime, as defined by $ka \gg 1$.

Continuing earlier research [7, 8], we consider electromagnetic waves illuminating one side of a perfectly-conducting plane screen comprising a set of slit apertures whose construction is mimicked by finitely many stages of a Cantor initiator-generator scheme. Since aperture domain intervals shrink exponentially, it does not always require many iterations until the condition $ka \ll 1$ dominates. The key physical issue to respect is that scattering from such irregular or finely-detailed structures can often constitute a low-frequency regime.

1.2 Fractal screens: the Cantor set

As a model for a fundamental fractal, we begin with the classic Cantor set [9]. The initiator stage (labelled by index $n = 0$) is simply the closed interval $C_0 := [0, 1]$ on the real line such that $C_0 \subset \mathbb{R}$. At the first stage ($n = 1$), the open middle third is removed to leave two subintervals and a new set $C_1 := C_0 \backslash (1/3, 2/3) = [0, 1/3] \cup [2/3, 1]$. At the second stage ($n = 2$), the open middle third of both subintervals is removed so that $C_2 = [0, 1/9] \cup [2/9, 3/9] \cup [6/9, 7/9] \cup [8/9, 9/9]$, and so on [see Fig. 1.1(a)]. After $n = 1, 2, 3, ...$ applications of this iterative process, one is left with $N_n = 2^n$ subintervals of finite length $l_n = 1/3^n$. In an intuitive Euclidean sense, one might define the 'length' of a particular set C_n by $L_n := N_n l_n = (2/3)^n$ implying that $L_\infty := \lim_{n\to\infty} L_n = 0$. More formally, one says that the the Cantor set $C_\infty := \lim_{n\to\infty} C_n$ has a Lebesque measure of zero; such a feature has implications for subsequent wave scattering problems.

The capacity dimension of C_∞ is given by

$$\dim_{\text{cap}}(C_\infty) = \lim_{n\to\infty} \frac{\log(N_n)}{\log(1/l_n)} = \lim_{n\to\infty} \frac{\log(2^n)}{\log(3^n)} = \frac{\log 2}{\log 3} \approx 0.631. \tag{1.1}$$

In a topological sense, then, the Cantor set has a tendency to fill space more efficiently than a point (whose Euclidean dimension is zero) but less efficiently than a regular line (Euclidean dimension one). A defining feature of any fractal set on the real line is that its capacity dimension falls within $(0, 1]$. Moreover, the Cantor set C_∞ possesses two striking properties: it is totally disconnected (like the integers) but also uncountable (like the reals).

Inspiration is now taken from the middle-third Cantor set to develop a model for pre-fractal plane screens [see Fig. 1.1(b)]. From $\mathbb{R}$, we remove the open interval $(-a_0, a_0)$ so that what remains is our initiator, $\Gamma_0 := \mathbb{R}\backslash(-a_0, a_0) = (-\infty, -a_0] \cup [a_0, \infty)$. Physically, the set Γ_0 may be interpreted as the screen in an idealized single-slit diffraction experiment [1, 3]. Now fill-in the closed middle third of the $[-a_0, a_0]$ interval to arrive at a set $\Gamma_1 := \Gamma_0 \cup [-a_0/3, a_0/3] = (-\infty, -a_0] \cup [-a_0/3, a_0/3] \cup [a_0, \infty)$. This time, Γ_1 denotes the domain of the screen for a symmetric double-slit experiment wherein the two apertures have equal width and separation, namely $2a_0/3$.

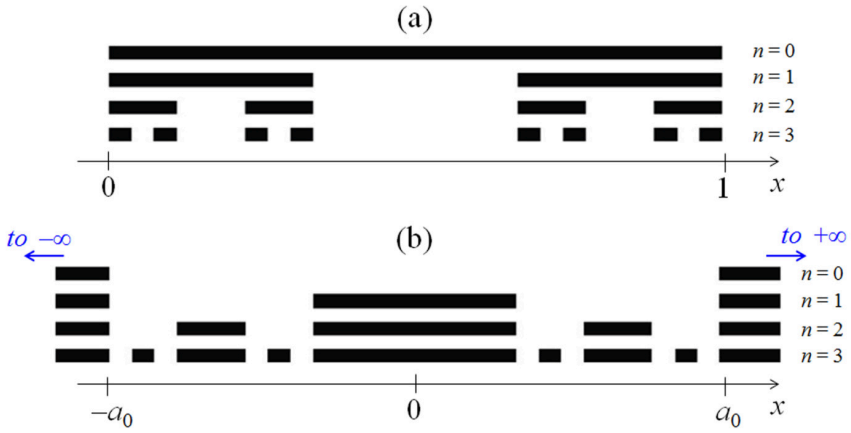

Figure 1.1: (a) Initiator ($n = 0$) and first three iterations ($n = 1, 2, 3$) of the classic middle-third Cantor set defined on the unit interval $[0, 1]$ of the real number line $\mathbb{R}$. (b) Iterative development of a pre-fractal Cantor screen. The domain of the opaque screen is Γ_n (black bars) while the domain of the transparent apertures (white bars) is $\overline{\Gamma} \subset (-a_0, a_0)$.

The iterative filling-in procedure may be repeated indefinitely to yield a set Γ_n that represents the domain of a screen comprising 2^n open apertures with width $2a_0/3^n$, where $n \in \mathbb{Z}_{\geq 0}$. The distribution of these apertures is contained within the $(-a_0, a_0)$ interval, and we denote that domain by $\overline{\Gamma}_n$. In the limit $n \to \infty$, the set Γ_∞ prescribes a plane Cantor fractal screen with uncountably many apertures of zero width.

The geometry of our scattering problem is shown in Fig. 1.2. The screen is translationally invariant along the z direction (out-of-page) and the electric field $\mathbf{E}(\mathbf{x}, t)$ everywhere in the surrounding space Ω is taken to be linearly polarized along z. We now introduce the standard decomposition for time-harmonic fields $\mathbf{E}(\mathbf{x}, t) = \hat{\mathbf{e}}_z[E_z(\mathbf{x}) \exp(-i\omega t) + \text{c.c.}]$, where $\hat{\mathbf{e}}_z$ denotes a unit vector in the z direction and ω is the angular frequency. Moreover, from Gauss's law and translational symmetry, we see that $\mathbf{E}$ cannot depend explicitly upon z. Position vectors are henceforth denoted by $\mathbf{x} = (x, y)$ so that (nominally) we may write $\Omega := \mathbb{R}^2 \backslash \Gamma_n$.

Dropping all reference to the z coordinate as an argument, the complex total field $E_z : \mathbb{R}^2 \to \mathbb{C}$ is now governed by the two-dimensional scalar Helmholtz equation

$$(\nabla^2 + k^2) E_z(\mathbf{x}) = 0 \quad \forall\ \mathbf{x} \in \Omega, \tag{1.2a}$$

where $\nabla^2 = \partial^2/\partial x^2 + \partial^2/\partial y^2$ is the Laplacian, $k = \omega/c$ is the wavenumber, and c is the vacuum speed of light. On the domain of a stage-n perfectly-conducting Cantor screen Γ_n, the boundary condition is of the homogeneous Dirichlet type [10],

$$E_z(\mathbf{x}) = 0 \quad \forall\ \mathbf{x} \in \Gamma_n, \tag{1.2b}$$

guaranteeing that the *total* electric field on the screen must vanish. To complete the picture, a plane wave $E_z^{\text{inc}}(\mathbf{x}) = E_\infty \exp(iky)$ with amplitude E_∞ and wavevector $\mathbf{k}_{\text{inc}} = \hat{\mathbf{e}}_y k$ is incident in the region $y < 0$, where $k = 2\pi/\lambda$.

1.3 A diffraction integral formulation

Our first objective is to calculate $E_z(\mathbf{x})$ in the region behind the screen, $y > 0$. That field will be referred to as the diffracted wave and labelled with the "diff" superscript. The free Green's

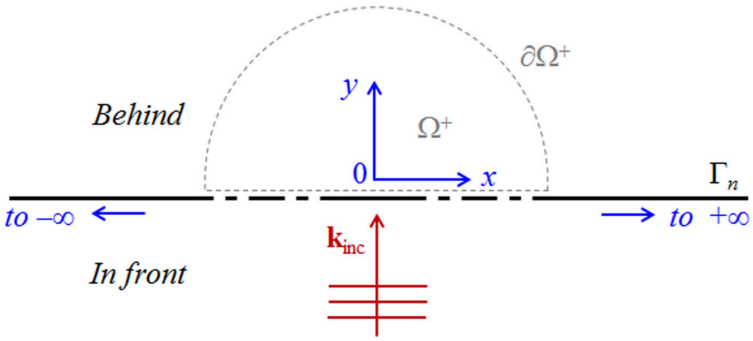

Figure 1.2: Geometry for normal-incidence wave scattering at a pre-fractal Cantor screen Γ_n (whose edges extend outwards toward ∞ and $-\infty$). For Eq. (1.4a), the boundary $\partial\Omega^+$ of region Ω^+ defined on the half-plane behind the screen is traversed in an anti-clockwise sense.

function for Eq. (1.2a), denoted by $G_0(\mathbf{x}|\mathbf{x}')$, satisfies the inhomogeneous equation [10]

$$(\nabla^2 + k^2)G_0(\mathbf{x}|\mathbf{x}') = -\delta(\mathbf{x} - \mathbf{x}'). \tag{1.3a}$$

The fundamental solution representing an outgoing cylindrical wave pertinent to our choice of decomposition for $\mathbf{E}(\mathbf{x}, t)$ must therefore be

$$G_0(\mathbf{x}|\mathbf{x}') = \frac{i}{4}H_0^{(1)}(k|\mathbf{x} - \mathbf{x}'|), \tag{1.3b}$$

where $H_0^{(1)}$ denotes the zero-order Hankel function of the first kind and we note the following symmetries for later use: $G_0(\mathbf{x}|\mathbf{x}') = G_0(|\mathbf{x} - \mathbf{x}'|) = G_0(\mathbf{x}'|\mathbf{x})$.

To facilitate analysis, consider a finite semicircular domain Ω^+ with boundary $\partial\Omega^+$ that is defined on $y > 0$ (see Fig. 1.2). We next follow Barton [11] to construct the Dirichlet Green's function $G_D(\mathbf{x}|\mathbf{x}') := G_0(\mathbf{x}|\mathbf{x}') + \chi(\mathbf{x}|\mathbf{x}')$ for a plane screen. If G_D is to also satisfy Eq. (1.3a), then the desired function χ should be a solution of $(\nabla^2 + k^2)\chi(\mathbf{x}|\mathbf{x}') = 0$. From the method of images, χ is determined to be $\chi(\mathbf{x}|\mathbf{x}') = -G_0(\mathbf{x}|\tilde{\mathbf{x}}')$ and where $\tilde{\mathbf{x}}'$ is a reflection of the source point $\mathbf{x}'$ about the line $y = 0$. Note that $\chi(\mathbf{x}|\mathbf{x}')$ is nowhere singular within the region of interest because $\tilde{\mathbf{x}}' \notin \Omega^+$.

Interchanging primed and unprimed variables, we proceed in the usual way to formulate an integral equation with reference to Green's second identity:

$$\begin{aligned}\iint_{\Omega^+} \mathrm{d}\Omega' \, \left[G_D(\mathbf{x}'|\mathbf{x})\nabla'^2 E_z^{\mathrm{diff}}(\mathbf{x}') - E_z^{\mathrm{diff}}(\mathbf{x}')\nabla'^2 G_D(\mathbf{x}'|\mathbf{x})\right] \\ = \oint_{\partial\Omega^+} \mathrm{d}\partial\Omega' \left[G_D(\mathbf{x}'|\mathbf{x})\frac{\partial E_z^{\mathrm{diff}}}{\partial n'}(\mathbf{x}') - E_z^{\mathrm{diff}}(\mathbf{x}')\frac{\partial G_D}{\partial n'}(\mathbf{x}'|\mathbf{x})\right],\end{aligned} \tag{1.4a}$$

where n' denotes the outward-normal direction to Ω^+. Substituting from Eqs. (1.2a) and (1.3a), the domain integration on the left-hand side of Eq. (1.4a) becomes

$$\iint_{\Omega^+} \mathrm{d}\Omega' \; \delta(\mathbf{x}' - \mathbf{x})E_z^{\mathrm{diff}}(\mathbf{x}') = \begin{cases} E_z^{\mathrm{diff}}(\mathbf{x}) & \mathbf{x} \in \Omega^+, \\ 0 & \mathbf{x} \notin \Omega^+. \end{cases} \tag{1.4b}$$

The boundary integration on the right-hand side of Eq. (1.4a) may be evaluated at any field point $\mathbf{x} \in \Omega^+$ once the input data $E_z^{\mathrm{diff}}(\mathbf{x}')$ and $(\partial/\partial n')E_z^{\mathrm{diff}}(\mathbf{x}')$ are specified on $\partial\Omega^+$. Since the

diffracted wave must respect the Sommerfeld radiation condition [11], falling off as

$$\lim_{r\to\infty} r^{1/2}\left(\frac{\partial E_z^{\rm diff}}{\partial r} - ikE_z^{\rm diff}\right) = 0, \tag{1.5}$$

the contribution to $E_z^{\rm diff}(\mathbf{x})$ from the semicircular portion of $\partial\Omega^+$ tends to zero as that boundary is taken out to infinity. Moreover, condition (1.5) guarantees there are no waves travelling inward from the far field. The remaining part of the boundary integration is along the straight-line base of the now-infinite semicircle, namely $x' \in (-\infty, \infty)$ and $y' = 0$. On that interval, the Dirichlet Green's function $G_D = 0$ (by construction) and its normal derivative has the properties

$$\frac{\partial G_D}{\partial n'}(\mathbf{x}'|\mathbf{x}) = 2\frac{\partial G_0}{\partial n'}(\mathbf{x}'|\mathbf{x}) = -2\frac{\partial G_0}{\partial y'}(\mathbf{x}'|\mathbf{x}). \tag{1.6}$$

Assembling all these results leads to the Rayleigh-Sommerfeld formula [1],

$$E_z^{\rm diff}(x,y) = i\frac{ky}{2}\int_{-\infty}^{\infty} {\rm d}x'\, E_z^{\rm diff}(x',0)\frac{1}{R}H_1^{(1)}(kR), \quad \text{where} \quad R := [(x-x')^2 + y^2]^{1/2} \tag{1.7a}$$

on $y > 0$. In the last step, we apply the St. Venant hypothesis [11] to enforce, in a 'weak' sense, input data for Eq. (1.7a) according to the prescription

$$E_z^{\rm diff}(x',0) = \begin{cases} 0 & x' \in \Gamma_n, \\ E_\infty & x' \in \overline{\Gamma}_n. \end{cases} \tag{1.7b}$$

In essence, condition (1.7b) anticipates that $E_z^{\rm diff}(x',0)$ adopts values identical to those of the incident plane wave $E_z^{\rm inc}(x', y' = 0) = E_\infty$ over each of the constituent aperture regions (a simplification routinely made in scalar diffraction theories [1, 2, 3]). Accommodating a stage-n Cantor screen, Eq. (1.7a) for the diffracted wave becomes

$$E_z^{\rm diff}(x,y) = iE_\infty\frac{ky}{2}\sum_{j=1}^{2^n}\int_{x_{0j}-a_0/3^n}^{x_{0j}+a_0/3^n} {\rm d}x'\,\frac{1}{R}H_1^{(1)}(kR), \tag{1.8}$$

where x_{0j} corresponds to the midpoint of aperture j in domain $\overline{\Gamma}_n$. We note, in passing, that exactly the same formula can be arrived at by Fourier-decomposing the diffracted wave on the $y > 0$ half-space and deploying the convolution theorem [1, 7]. The remaining two Cartesian components of the diffracted electric-field vector are rigorously zero so that $E_x^{\rm diff}(x,y) = 0 = E_y^{\rm diff}(x,y)$ and hence $\mathbf{E}^{\rm diff}(x,y) = (0, 0, E_z^{\rm diff}(x,y))$.

The corresponding diffraction integral from Fresnel optics [3] can be recovered from an asymptotic expansion of the kernel in Eq. (1.8) for large arguments $kR \gg 1$ [12]. By making the small-angle approximation within the phase factor kR and anticipating that the amplitude factor $1/R$ is constant across the region of integration, we obtain

$$E_z^{\rm diff}(x,y) \approx E_\infty\left(\frac{k}{i2\pi y}\right)^{1/2}\exp(iky)\sum_{j=1}^{2^n}\int_{x_{0j}-a_0/3^n}^{x_{0j}+a_0/3^n} {\rm d}x'\,\exp\left[i\frac{k}{2y}(x-x')^2\right]. \tag{1.9a}$$

For a stage-n Cantor screen, Eq. (1.9a) might be expected to hold (at least in a high-frequency regime) for distances that satisfy $y \gg [(ka_0^4/8)/81^n]^{1/3}$. Each constituent integral may be

couched in terms of a pair of Young's edge waves [3]. After defining the change-of-variables $s := (k/\pi y)^{1/2}(x - x')$, and without making further approximation, Eq. (1.9a) is recast as

$$E_z^{\text{diff}}(x,y) \approx E_\infty \left(\frac{1}{i2}\right)^{1/2} \exp(iky) \sum_{j=1}^{2^n} \int_{s_j(x,y;n_-)}^{s_j(x,y;n_+)} \mathrm{d}s \, \exp\left(i\frac{\pi}{2}s^2\right),$$

$$= E_\infty \exp(iky) \sum_{j=1}^{2^n} \Big[\psi(s_j(x,y;n_+)) - \psi(s_j(x,y;n_-))\Big], \tag{1.9b}$$

where we have introduced $s_j(x,y;n_\pm) = (k/\pi y)^{1/2}(x - x_{0j} \pm a_0/3^n)$ for the limits of integration followed by the edge wave $\psi(\chi) = -(i/2)^{1/2}\phi^*(\chi)\exp[i(\pi/2)\chi^2]$. Here, $\phi : \mathbb{R} \to \mathbb{C}$ is a complex linear combination of the auxiliary Fresnel functions which themselves can be computed quickly and efficiently by deploying suitable rational approximations [13, 14].

In the far field, wavefront curvature is neglected in the x' coordinate of Eq. (1.9a) and the Fourier integrals that result may be evaluated exactly to yield

$$E_z^{\text{diff}}(x,y) \approx E_\infty \left(\frac{k}{i2\pi y}\right)^{1/2} \exp\left[i\left(ky + \frac{kx^2}{2y}\right)\right] \frac{2a_0}{3^n} \text{sinc}\left(\frac{Ka_0}{3^n}\right) \sum_{j=1}^{2^n} \exp(-iKx_{0j}), \tag{1.10}$$

where $K := kx/y$. The far-field solution thus comprises a linear superposition of 2^n single-slit patterns, and where the strength of the diffracted wave can be expected to decay with n such that $E_z^{\text{diff}}(x,y) \to 0$ as $n \to \infty$ (since the interval being integrated over in x' approaches zero).

Formally, the diffracted magnetic flux density vector $\mathbf{B}^{\text{diff}}(x,y)$ is obtained from Maxwell's equations via Faraday's law, $\mathbf{B}^{\text{diff}}(x,y) = (ick)^{-1}\nabla \times \mathbf{E}^{\text{diff}}(x,y)$. In component form,

$$B_x^{\text{diff}}(x,y) = \frac{1}{ick}\frac{\partial E_z^{\text{diff}}}{\partial y}(x,y), \quad B_y^{\text{diff}}(x,y) = -\frac{1}{ick}\frac{\partial E_z^{\text{diff}}}{\partial x}(x,y), \quad \text{and} \quad B_z^{\text{diff}}(x,y) = 0 \tag{1.11a}$$

so that, upon differentiation, we obtain [7]

$$B_x^{\text{diff}}(x,y) = \frac{B_\infty}{2} \sum_{j=1}^{2^n} \int_{x_{0j}-a_0/3^n}^{x_{0j}+a_0/3^n} \mathrm{d}x' \, \frac{1}{R}\left[H_1^{(1)}(kR) - ky\left(\frac{ky}{R}\right)H_2^{(1)}(kR)\right], \tag{1.11b}$$

$$B_y^{\text{diff}}(x,y) = B_\infty \frac{ky}{2} \sum_{j=1}^{2^n} \int_{x_{0j}-a_0/3^n}^{x_{0j}+a_0/3^n} \mathrm{d}x' \, \frac{1}{R^2}(x - x')H_2^{(1)}(kR), \tag{1.11c}$$

where $B_\infty := E_\infty/c$. Having derived all the electric and magnetic components of the diffracted wave, it is a straightforward exercise to establish that the vector fields $\mathbf{E}^{\text{diff}}(x,y)$ and $\mathbf{B}^{\text{diff}}(x,y)$ are divergence-free, as should be the case. That is, $\nabla \cdot \mathbf{E}^{\text{diff}}(x,y) = 0$ and $\nabla \cdot \mathbf{B}^{\text{diff}}(x,y) = 0 \; \forall \; x, y \in \Omega^+$.

Examples of electromagnetic waves scattered by pre-fractal Cantor screens, as predicted by Eqs. (1.7a), (1.11b), and (1.11c) are given in Fig. 1.3 for the case of $2a_0 = 20\lambda$. At $n = 0$, one has $ka_0 = 20\pi \approx 62.83$ and so the Rayleigh-Sommerfeld solution is arguably valid. Diffraction is fairly weak since, in the region close behind the screen, the wave spreads out hardly at all. For $n = 4$, one instead has $ka_4 = ka_0/3^4 \approx 0.78$. Diffraction is evidently stronger in this much lower-frequency regime. Here, one must be mindful that predictions made by a Rayleigh-Sommerfeld formulation are likely not faithful to the true (physical) solutions otherwise obtained from Maxwell's equations.

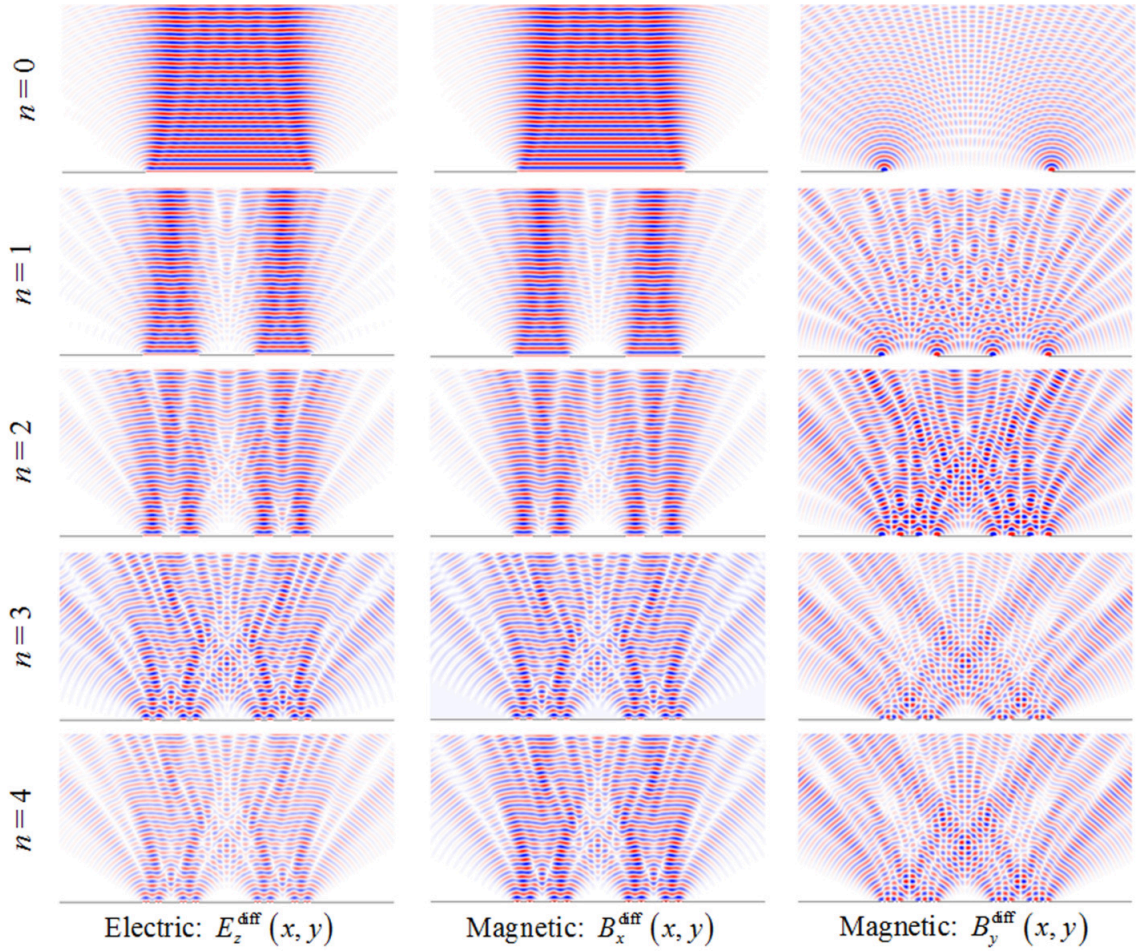

Figure 1.3: Snapshot at time $t = 0$ of diffracted electromagnetic waves for a set of pre-fractal Cantor screens as predicted by Eqs. (1.8), (1.11b), and (1.11c). The initiator aperture is chosen to be $2a_0 = 20\lambda$. Note that $B_x^{\text{diff}}(x, y)$ is the dominant component of the magnetic flux density.

To reconstruct the total electromagnetic field within the entire space Ω, symmetries inherent to the plane-screen class of problem may be exploited [10]. Behind the screen, where $y > 0$, only the diffracted wave exists: one has simply $\mathbf{E}(x, y) = \mathbf{E}^{\text{diff}}(x, y)$ and $\mathbf{B}(x, y) = \mathbf{B}^{\text{diff}}(x, y)$. In front of the screen, where $y < 0$, account must be taken of the incident and reflected waves. Recalling that $\mathbf{E}^{\text{inc}}(\mathbf{x}) = \hat{\mathbf{e}}_z E_\infty \exp(iky) \implies \mathbf{B}^{\text{inc}}(\mathbf{x}) = \hat{\mathbf{e}}_x B_\infty \exp(iky)$, we have

$$E_z(x, -y) = E_\infty \exp(iky) - E_\infty \exp(-iky) + E_z^{\text{diff}}(x, y), \tag{1.12a}$$

$$B_x(x, -y) = B_\infty \exp(iky) + B_\infty \exp(-iky) - B_x^{\text{diff}}(x, y), \tag{1.12b}$$

$$B_y(x, -y) = B_y^{\text{diff}}(x, y). \tag{1.12c}$$

In this way, diffraction integral equation (1.7a) in conjunction with the St. Venant hypothesis (1.7b) has been used to compute the electromagnetic field in the entire space surrounding a plane pre-fractal Cantor screen. Note the appearance of the standing wave in front of the screen, arising from the interference between incident and reflected waves as captured by Eqs. (1.12a) and (1.12b). This feature has been included *a posteriori* for the diffraction-integral solution, but we will see shortly that it appears naturally as part of the boundary element method.

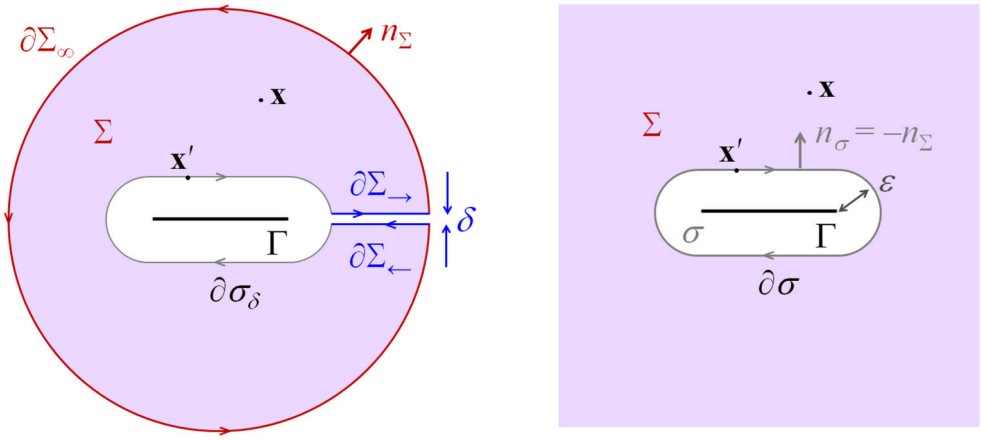

Figure 1.4: Domain decomposition for formulating boundary integral equation (1.14a). Left: The boundary $\partial\Sigma$ is constructed according to $\partial\Sigma = \partial\Sigma_\infty \cup \partial\Sigma_\leftarrow \cup \partial\sigma_\delta \cup \partial\Sigma_\rightarrow$. Right: The region σ enclosing the strip Γ has a boundary $\partial\sigma$ on which the outward normal is $n_\sigma = -n_\Sigma$.

1.4 Towards a boundary element method

We now turn our attention to formulating a boundary element description of a related scattering problem. There are some basic similarities with the diffraction integral approach, but the focus is naturally on respecting full Dirichlet boundary conditions. To proceed, the total electric field $E_z(\mathbf{x})$ is decomposed into a linear superposition of the incident wave and the scattered wave according to

$$E_z(\mathbf{x}) = E_z^{\text{inc}}(y) + E_z^{\text{sc}}(\mathbf{x}) \;\; \forall \;\; \mathbf{x} \in \Omega. \tag{1.13a}$$

Compare this situation to the Rayleigh-Sommerfeld approach, where the incident wave exists only on the half-space $y < 0$ and the diffracted wave only on $y > 0$. Both contributions to decomposition (1.13a) satisfy Eq. (1.2a) independently. Also, since the total electric field on the Cantor screen Γ_n must still vanish [as per Eq. (1.2b)], the scattered wave $E_z^{\text{sc}}(\mathbf{x})$ is instead subject to the inhomogeneous Dirichlet boundary condition

$$E_z^{\text{sc}}(\mathbf{x}) = -E_\infty \;\; \forall \, \mathbf{x} \in \Gamma_n. \tag{1.13b}$$

Moreover, E_z^{sc} is also constrained by the Sommerfeld radiation condition [akin to Eq. (1.5)].

As a starting point, we will consider only the scattering from an arbitrary finite interval Γ (no subscript index) that forms part of a given stage-n Cantor screen Γ_n. Physically, Γ may be interpreted as a perfectly-conducting thin strip aligned along the z axis [15, 16]. For an arbitrary surrounding domain Σ with simple closed boundary $\partial\Sigma$ and outward normal n_Σ, a Green's integral equation involving $E_z^{\text{sc}}(\mathbf{x})$ and $G_0(\mathbf{x}|\mathbf{x}')$ may be derived such that

$$a(\mathbf{x}) E_z^{\text{sc}}(\mathbf{x}) = \oint_{\partial\Sigma} \mathrm{d}\partial\Sigma' \left[G_0(\mathbf{x}'|\mathbf{x}) \frac{\partial E_z^{\text{sc}}}{\partial n'_\Sigma}(\mathbf{x}') - E_z^{\text{sc}}(\mathbf{x}') \frac{\partial G_0}{\partial n'_\Sigma}(\mathbf{x}'|\mathbf{x}) \right]. \tag{1.14a}$$

The factor $a(\mathbf{x})$, which originates in an integration across a Dirac delta function, is given by $a(\mathbf{x}) = 1$ for $\mathbf{x} \in \Sigma$, $1/2$ for $\mathbf{x} \in \partial\Sigma$ (smooth boundary), and 0 for $\mathbf{x} \notin \Sigma$.

Equation (1.14a) holds for arbitrary Σ, which may be freely deformed into any desired shape. Choosing Σ as shown in Fig. 1.4 has a two-fold purpose. First, as the outer circular boundary

$\partial\Sigma_\infty$ tends to infinity, the Sommerfeld condition guarantees that there is no contribution to $E_z^{\rm sc}(\mathbf{x})$. Second, as the gap size $\delta \to 0$, contributions from the incoming and outgoing paths cancel (since the outward normals along $\partial\Sigma_\leftarrow$ and $\partial\Sigma_\rightarrow$ point in opposite directions). The only surviving contribution to the circulation in Eq. (1.14a) is from the inner boundary $\partial\sigma := \partial\sigma_\delta|_{\delta\to 0}$, which has an outer normal $n_\sigma := -n_\Sigma$. As $\epsilon \to 0$, the contribution from the two semicircular end-caps vanishes to leave an integration out (over the upper surface: $\partial/\partial n'_\sigma = \partial/\partial y'$) and back (over the lower surface: $\partial/\partial n'_\sigma = -\partial/\partial y'$) along Γ:

$$a(\mathbf{x})E_z^{\rm sc}(\mathbf{x}) = \int_{-b}^{b} \mathrm{d}x' \left[E_z^{\rm sc}(x',0)\frac{\partial G_0}{\partial y'}(\hat{\mathbf{e}}_x x'|\mathbf{x}) - G_0(\hat{\mathbf{e}}_x x'|\mathbf{x})\frac{\partial E_z^{\rm sc}}{\partial y'}(x',0)] \right]. \tag{1.14b}$$

Domain $\sigma|_{\epsilon\to 0}$ coincides with strip Γ, taken here to have a width $2b$ centred on the origin of the x' coordinate.

Boundary integral equation (1.14b) represents the scattered field $E_z^{\rm sc}(\mathbf{x})$ at any point $\mathbf{x} \in \mathbb{R}^2\backslash\Gamma$ as arising from a distribution of free Green's-function sources over domain Γ. For the inhomogeneous Dirichlet problem, condition (1.13b) implies that $E_z^{\rm sc}(x',0) = -E_\infty \; \forall \; x' \in [-b,b]$. The goal is thus to obtain an approximation for the remaining input data, namely $(\partial/\partial y')E_z^{\rm sc}(x',0)$, by devising a boundary element scheme.

The discretization procedure represents Γ by N equally-spaced nodes and the strip thus comprises $N-1$ elements of finite size $l = L/(N-1)$. On Γ, we make the replacements

$$E_z^{\rm sc}(x',0) \to \sum_{q=1}^{N} E_q N_q(x') \quad \text{and} \quad \frac{\partial E_z^{\rm sc}}{\partial y'}(x',0) \to \sum_{q=1}^{N} F_q N_q(x'), \tag{1.15}$$

where E_q and F_q with $q = 1,2,3,...,N$ are two sets of constants specifying the input data. For simplicity, $N_q(x')$ is taken as a standard piecewise-linear shape function. Qualitatively, $N_q(x')$ resembles a unit-height isosceles triangle whose base spans the element either side of node q, and is equal to zero otherwise [17].

Equation (1.14b) may be evaluated on the strip by setting the field point $\mathbf{x} = (x,y) \to (\xi,0)$, where $\xi \in [-b,b]$. In point collocation, the role of a weighting function such as

$$w_p(\xi) = \delta(\xi - \xi_p) \tag{1.16}$$

is to place a Green's-function source at the position ξ_p of node $p = 1,2,3,...,N$. Evaluating on Γ, we multiply Eq. (1.14b) throughout by $w_p(\xi)$ and integrate over the domain so that

$$\begin{aligned}\int_{-b}^{b} \mathrm{d}\xi\, w_p(\xi) \left[\sum_{q=1}^{N} E_q a(\xi) N_q(\xi) \right] &= \int_{-b}^{b} \mathrm{d}\xi\, w_p(\xi) \left[\sum_{q=1}^{N} E_q \int_{-b}^{b} \mathrm{d}x' N_q(x') \frac{\partial G_0}{\partial y'}(x'|\xi) \right] \\ &- \int_{-b}^{b} \mathrm{d}\xi\, w_p(\xi) \left[\sum_{q=1}^{N} F_q \int_{-b}^{b} \mathrm{d}x'\, N_q(x') G_0(x'|\xi) \right]. \end{aligned} \tag{1.17a}$$

Interchanging the summations and integrations gives

$$\begin{aligned}\sum_{q=1}^{N} E_q \left[\int_{-b}^{b} \mathrm{d}\xi\, \delta(\xi-\xi_p) a(\xi) N_q(\xi) \right] &= \sum_{q=1}^{N} E_q \int_{-b}^{b} \mathrm{d}x'\, N_q(x') \left[\int_{-b}^{b} \mathrm{d}\xi\, \delta(\xi-\xi_p) \frac{\partial G_0}{\partial y'}(x'|\xi) \right] \\ &- \sum_{q=1}^{N} F_q \int_{-b}^{b} \mathrm{d}x'\, N_q(x') \left[\int_{-b}^{b} \mathrm{d}\xi\, \delta(\xi-\xi_p) G_0(x'|\xi) \right], \end{aligned} \tag{1.17b}$$

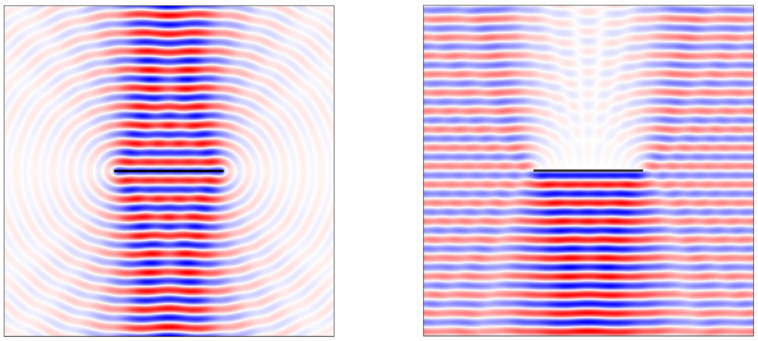

Figure 1.5: Numerical computation from our boundary element method on a square grid $(x, y) \in [-9\lambda, 9\lambda] \times [-9\lambda, 9\lambda]$ for a strip $2b = 6\lambda$. Left: Scattered wave $\mathrm{Re}[E_z^{\mathrm{sc}}(x, y)]$. Right: Physical electric field $E_z(x, y, t)$ reconstructed from Eq. (1.13a) at time $t = T/4$, where $T = 2\pi/\omega$.

and subsequently evaluating the ξ integrals (with recourse to the sifting property of Dirac delta functions) leaves

$$\sum_{q=1}^{N} E_q a(\xi_p) N_q(\xi_p) = \sum_{q=1}^{N} E_q \int_{-b}^{b} \mathrm{d}x'\, N_q(x') \frac{\partial G_0}{\partial y'}(x'|\xi_p) - \sum_{q=1}^{N} F_q \int_{-b}^{b} \mathrm{d}x'\, N_q(x') G_0(x'|\xi_p). \quad (1.17c)$$

From inspection, we see that there can be no contribution from the first term on the right-hand side of Eq. (1.17c) because the normal derivative of G_0 is necessarily zero on the domain:

$$\frac{\partial G_0}{\partial y'} = \hat{\mathbf{e}}_y \cdot \nabla' G_0(\mathbf{x}'|\mathbf{x}) = -i\frac{k}{4} H_1^{(1)}(k|\mathbf{x}' - \mathbf{x}|) \frac{\hat{\mathbf{e}}_y \cdot (\mathbf{x}' - \mathbf{x})}{|\mathbf{x}' - \mathbf{x}|} = 0 \ \text{ on } \ \Gamma \quad (1.17d)$$

since $\mathbf{x}' - \mathbf{x} = \hat{\mathbf{e}}_x(x' - \xi) + \hat{\mathbf{e}}_y 0 \implies \hat{\mathbf{e}}_y \cdot (\mathbf{x}' - \mathbf{x}) = 0 \ \forall \ \mathbf{x}', \mathbf{x} \in \Gamma$. For the second term, it is instructive to introduce the set of entries for a dense matrix $A \in \mathbb{C}^{N \times N}$ according to

$$A_{pq} := \int_{-b}^{b} \mathrm{d}x'\, N_q(x') G_0(x'|\xi_p) = \frac{i}{4} \int_0^l \mathrm{d}l'\, \frac{l'}{l} H_0^{(1)}(k|l' + \xi_{q-1} - \xi_p|) + \frac{i}{4} \int_0^l \mathrm{d}l' \left(1 - \frac{l'}{l}\right) H_0^{(1)}(k|l' + \xi_q - \xi_p|). \quad (1.18a)$$

For each index combination (p, q), the integration typically extends over a pair of consecutive boundary elements (we forego a discussion of the endpoints here).

This formulation is quite general in that no boundary condition has yet been imposed. For the scattering-from-a-strip scenario, and with reference to Eq. (1.13b), we stipulate $E_q = -E_\infty \ \forall \ q$ and set $a(\xi_p) = 1/2 \ \forall \ p$. The remaining unknowns are the F_q's, and they can be determined by first formulating the set of N linear algebraic equations

$$\sum_{q=1}^{N} A_{pq} F_q = Y_p, \ \text{ where } \ Y_p := \frac{E_\infty}{2} \sum_{q=1}^{N} N_q(\xi_p) \quad (1.18b)$$

defines the entries of a column vector $Y = \mathrm{col}(Y_1, Y_2, Y_3, ..., Y_N) \in \mathbb{C}^{N \times 1}$. One computes the desired column vector comprising the boundary data, $F = \mathrm{col}(F_1, F_2, F_3, ..., F_N) \in \mathbb{C}^{N \times 1}$, by solving numerically the matrix inversion problem $F = A^{-1}Y$ (with recourse to the Moore-Penrose pseudo-inverse). Once F has been obtained, it is straightforward to reconstruct $E_z^{\mathrm{sc}}(\mathbf{x}) \ \forall \ \mathbf{x} \in \mathbb{R}^2 \backslash \Gamma$ by discretizing Eq. (1.14b). A result is shown in Fig. 1.5 for the case of $2b = 6\lambda$.

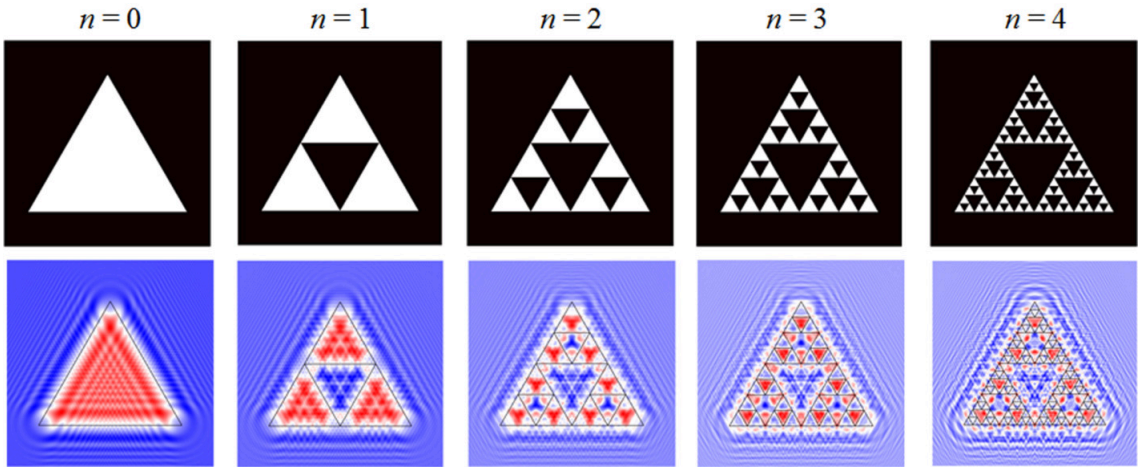

Figure 1.6: Rayleigh-Sommerfeld calculations [1, 8] (in the near field) of the diffracted wave from pre-fractal screens based on iterations of the Sierpinski triangle [9].

1.5 Discussion

Our research is focusing on boundary element formulations to describe electromagnetic waves scattering from perfectly-conducting pre-fractal plane screens. This more powerful approach avoids the approximations inherent to the diffraction integrals traditionally encountered in laser optics [3]. The starting point has been an analysis of the infinitely-long perfectly-conducting thin strip with finite width. When the incident electric-field vector is linearly polarized along the length of the strip, the corresponding boundary-value problem is of the (inhomogeneous) Dirichlet type. The strip can be regarded as a 'building block' for decomposing the domain of a pre-fractal screen based on the Cantor set. It is also of interest in its own right (e.g., in the context of Babinet's principle and scattering by complementary screens [10, 18]).

Our preliminary work in the realm of electromagnetic scattering has connections to much further developed research by Chandler-Wilde *et al.* [19, 20, 21], where rigorous functional analysis and boundary integral methods have been applied to acoustic scattering on pre-fractal and fractal screens.

Topics to be addressed in our future research include: (i) incorporation of infinite boundary elements [17], (ii) a detailed comparison with the corresponding Rayleigh-Sommerfeld predictions, (iii) full exploration of how boundary conditions determine details of the scattered wave [e.g., transverse-electric *Dirichlet* and transverse-magnetic Neumann problems], (iv) an analysis of Babinet's principle in a full electromagnetic context, and (v) application to pre-fractal screens with two non-trivial transverse dimensions; typical examples include von Koch snowflake-type shapes, Sierpinski (see Fig. 1.6) and Apollonian gaskets, and Cantor dusts [7, 8].

References

[1] Stamnes J. J. *Waves in Focal Regions: Propagation, Diffraction and Focusing of Light, Sound and Water Waves*, IoP Publishing, UK, 1986.

[2] Marathay A. S. and McCalmont J. F. On the usual approximation used in the Rayleigh-Sommerfeld diffraction theory. *Journal of the Optical Society of America A*, 21(4): 510–516, 2004.

[3] Siegman A. E. *Lasers*, University Science Books, USA, 1986.

[4] Allain C. and Cloitre M. Optical diffraction on fractals. *Physical Review B*, 33(5): 3566–3569, 1986.

[5] Saavedra G., Furlan W. D., and Monsoriu J. A. Fractal zone plates. *Optics Letters*, 28(12): 971–973, 2003.

[6] Hou B., Xu. G., Wen. W., and Wong G. K. L. Diffraction by an optical fractal grating. *Applied Physics Letters*, 85(25): 6125–6127, 2004.

[7] Middleton-Spencer H. A. J. *The diffraction of monsters from complex apertures: towards an electromagnetic approach.* MSc thesis, University of Salford, Greater Manchester, UK, 2018.

[8] Christian J. M. and Middleton-Spencer H. A. J. *On the scattering of electromagnetic waves by fractal screens: a Rayleigh-Sommerfeld approach.* Institute of Mathematics and its Applications (invited talk), University of Manchester, UK, 2018.

[9] Falconer K. J. *Fractal Geometry: Mathematical Foundation and Applications*, 3rd ed., John Wiley & Sons, UK, 2014.

[10] Jackson J. D. *Classical Electrodynamics*, 3rd ed., John Wiley & Sons, USA, 1999.

[11] Barton G. *Elements of Green's Functions and Propagation: Potentials, Diffusion and Waves*, Oxford University Press, UK, 2005.

[12] Abramowitz M. and Stegun I. A. *Handbook of Mathematical Functions with Formulas, Graphs, and Mathematical Tables*, 9th ed., Dover, USA, 1964.

[13] Huang J. G., Christian J. M., and McDonald G. S. Fresnel diffraction and fractal patterns from polygonal apertures. *Journal of the Optical Society of America A*, 23(11): 2768–2774, 2006.

[14] Heald M. A. Rational approximations for the Fresnel integrals. *Mathematics of Computation*, 44(170): 459–461, 1985.

[15] Barkeshli K. and Volakis J. L. Electromagnetic scattering from thin strips—Part I: Analytical solutions for wide and narrow strips. *IEEE Transactions on Education*, 47(1): 100–106, 2004.

[16] Barkeshli K. and Volakis J. L. Electromagnetic scattering from thin strips—Part II: Numerical solution for strips of arbitrary size. *IEEE Transactions on Education*, 47(1): 107–113, 2004.

[17] Chadwick E. A. A boundary element formulation for the tripe decks of high Reynolds number flow past a finite flat plate. *Proceedings of the 14th UK Conference on Boundary Integral Methods (UKBIM14)*, University of Salford, Greater Manchester, UK, 2025.

[18] Brooker G. A. Diffraction at a single ideally conducting slit. *Journal of Modern Optics*, 55(3): 423–445, 2008.

[19] Chandler-Wilde S. N. and Hewett D. P. Well-posed PDE and integral equation formulations for scattering by fractal screens. *SIAM Journal on Mathematical Analysis*, 50(1): 677–717, 2018.

[20] Chandler-Wilde S. N., Hewett D. P, and Moila A. Sobolev spaces on non-Lipschitz subsets of $\mathbb{R}^n$ with application to boundary integral equations on fractal screens. *Integral Equations and Operator Theory*, 87: 179–224, 2017.

[21] Hewett D. P., Langdon S., and Chandler-Wilde S. N. A frequency-independent boundary element method for scattering by two-dimensional fractal screens and apertures. *IMA Journal of Numerical Analysis*, 35: 1698–1728, 2015.